Performance of molten sodium vs. molten salts in a packed bed thermal energy storage

Klarissa Niedermeier[a,*], Luca Marocco[b], Jonathan Flesch[a], Gowtham Mohan[c], Joe Coventry[c], Thomas Wetzel[a]

[a]*Karlsruhe Institute of Technology (KIT), Institute for Nuclear and Energy Technologies, Hermann-von-Helmholtz-Platz 1, 76344 Eggenstein-Leopoldshafen, Germany*
[b]*Politecnico di Milano, Department of Energy, via Lambruschini 4, 20156 Milan, Italy*
[c]*Australian National University (ANU), Research School of Engineering, Canberra, ACT 0200, Australia*

Abstract

Concentrating solar power plants are currently working with Solar Salt and conventional Rankine steam power cycles with upper temperatures of $565\,°C$. To achieve higher efficiencies, advanced power cycles are currently investigated ($500\,°C$ to $700\,°C$). As heat transfer fluids, both molten sodium and three types of molten salt are considered in this study. For power tower plants, the heat transfer fluid is typically also the storage medium. This is the case for state-of-the-art commercial plants using molten salt, and past and present pilot plants using sodium. However, this work shows for both cases that a packed bed arrangement, where the heat transfer fluid is replaced by a filler material, may be a technically feasible and economically viable alternative. Furthermore, for sodium there are additional safety concerns related to having a large sodium inventory, which the packed bed arrangement can help alleviate. In this study, a $40\,MWh_{th}$ storage system with quartzite as filler material is numerically investigated with a one-dimensional model. The results are evaluated in terms of discharge efficiency, pumping power, storage cost and thermocline degradation during standby to assess the potential of this storage solution for future scientific investigations. The packed bed system with sodium shows slightly higher discharge efficiencies ($96.8\,\%$) than with molten salt ($95.2\text{-}95.7\,\%$) and also lower required pumping power. However, the thermocline region expands faster during standby due to the high thermal conductivity of sodium. The influence of porosity, tank diameter-to-height ratio and filler particle diameter is analysed in a parametric study. Highest discharge efficiencies are achieved for both sodium and molten salts with small tank diameter-to-height ratios and small filler particles. For sodium, low porosities are preferable, while for molten salts, high porosities lead to better discharge efficiencies.

Keywords: liquid metal, sodium, thermal energy storage, thermocline, packed bed

1. Introduction

Operational concentrating solar thermal power plants like Gemasolar or Crescent Dunes use a $NaNO_3$-KNO_3 mixture (composition by weight 0.60-0.40) called 'Solar Salt' as the heat transfer fluid (HTF) and as the storage medium. To increase the efficiency of central receiver systems, advanced power cycles with higher upper temperature limits are currently considered [1], [2]. However, the operating temperature range of Solar Salt is limited by its decomposition temperature ($\approx 600\,°C$). For higher temperatures, alternative HTF candidates are proposed.
A review by Pacio et al. [3] shows that liquid metals (e.g. sodium, lead-bismuth-eutectic, sodium-potassium and tin) might qualify as attractive HTFs, because of their excellent heat transfer properties. Among these, sodium stands out due to its low melting point and high boiling temperature. Sodium has already been tested as HTF at the

IEA-SSPS central receiver facility in Almeria, Spain, during the 1980s [4] and currently in a pilot-scale ($1\,MW_e$) plant at Jemalong, Australia [5]. However, its comparably low volumetric thermal capacity ($\rho_f c_{pf}$) and high cost do not advertise it as storage fluid in a direct two-tank configuration, as is currently applied in operational solar tower plants with molten salts. Furthermore, sodium reacts exothermally in contact with air and water. However, with the high standards of safety inherited from the long term nuclear industrial experience, these risks can be minimized [6]. Therefore, a thermocline packed-bed thermal energy storage system is suggested, leading to less sodium inventory, higher storage densities and lower storage material cost, as shown by Niedermeier et al. [7].

On the other hand, alternative salt compositions are also considered as HTFs for advanced power cycles. These are not only interesting due to higher decomposition temperatures compared to the commonly used Solar Salt, but also due to their applicability as storage media. The main disadvantage is their relatively high melting temperature, which makes extensive heat tracing inevitable. The Con-

*Corresponding author
Email address:* k.niedermeier@kit.edu (Klarissa Niedermeier)

centrating Solar Power Gen3 Demonstration Roadmap [8] suggests three main canditate salt mixtures: $ZnCl_2$-NaCl-KCl (composition by weight 0.686-0.075-0.239), $MgCl_2$-KCl (composition by weight 0.375-0.625) and Na_2CO_3-K_2CO_3-Li_2CO_3 (composition by weight 0.334-0.345-0.321). The chloride salts are already very low in price, but a single-tank packed bed system with cheap filler material could lead to even further reduced cost. Additionally, one tank is used rather than two, which means more than 25 % investment cost reduction due to the reduced tank material [9]. In this study, these three salts are compared to sodium as HTFs in a packed bed thermocline storage system.

Quartzite (SiO_2) spheres are taken as examplary packed bed material. Chemical compatibility issues with the HTFs in the considered temperature range are not considered in this study. Further filler material candidates are listed in a review by Esence et al. [10].

The technical feasiblity of thermocline storage systems with filler material has been demonstrated in several projects in the past. A thermocline storage with granite rocks and sand as filler material and oil as HTF was used in the first large-scale power tower test plant, Solar One, in the 1980s [11]. Furthermore, Pacheco et al. [12] performed experiments on a pilot-scale plant with Solar Salt as HTF and a quarzite rock and sand mixture as filler material. Recently, the German Aerospace Center (DLR) has put a pilot-scale facility into operation for demonstration and material studies of a thermocline storage with salt mixtures and filler material [13].

However, a liquid metal thermocline storage system with filler material has rarely been reported in the literature, neither theoretically nor experimentally. Pomeroy et al. [14] proposed a packed bed of iron spheres with sodium as the HTF in the 1980s. To the authors' best knowledge, no further investigations have been performed since.

Therefore, a comparison of high temperature salts and sodium as HTFs in a packed bed system is performed in this work based on a one-dimensional two-phase simulation. Firstly, a review of performance comparisons of thermocline storage systems in the literature is conducted (Section 2). The methodology for the comparison in this work is introduced (Section 3) and the numerical model is presented (Section 4). Finally, the results of the comparison are discussed (Section 5) and summarised (Section 6).

2. Review: Performance comparison of thermocline storage systems

In the literature, the performances of different HTFs in thermocline storage systems with filler material are compared based on numerical studies. However, the reference cases and definitions of storage efficiency used are not always consistent.

Modi et al. [15] compare Solar Salt, HITEC and Therminol 66. The reference case is a 5 h storage system with fixed tank dimensions and two selected maximum temperatures (390 °C and 560 °C). The remaining storage parameters (fluid velocity, particle size and porosity) are taken from Pacheco et al. [12]. They show the temperature profiles at the beginning and at the end of one discharge cycle and evaluate the efficiency based on the temperature distribution along the tank height and on the storage capacity after discharging. The latter is defined as the total accumulated thermal energy in the tank (by filler and fluid). However, as only the dimensions of the tanks are fixed and not the total initial storage capacity, Therminol 66 and HITEC have smaller initial storage capacities than Solar Salt. Their comparison concludes that, both regarding stratifiction and storage capacity, best results can be accomplished with Solar Salt, followed by HITEC and Therminol 66.

Cascetta et al. [16] choose air, Therminol VP-1 and Solar Salt as HTFs for their comparison. The reference case is a 5 h storage system with a fixed storage capacity of $5\,MWh_{th}$. Different lower and upper temperature limits are defined for each fluid, which results in different tank sizes and fluid velocities for each fluid. The authors define the storage efficiency as the ratio of storage capacity after each cycle to the "maximum energy". This "maximum energy" is the initial storage capacity of the system, which is the same for all fluids. They find the highest efficiency for Solar Salt, however, only the first 5 cycles are shown and the storage efficiency does not appear to have stabilised.

Vilella and Yesilyurt [17] compare the discharge efficiency of Solar Salt, HITEC XL and Therminol as HTFs in a packed bed storage with a capacity based on Andasol 1 ($1\,GWh_{th}$). The operating temperature limits are 291 °C and 384 °C to guarantee that all fluids are liquid at any time. The definition of the storage efficiency is the ratio of energy extracted during discharge related to the energy of an ideal discharge. At first, they compare with constant mass flow concluding that Solar Salt is the best performing HTF. However, they state that a fairer comparison should be based on the "thermal mass flow rate" ($\dot{m}c_{pf}$). This leads to similar efficiencies for all investigated HTFs. Additionally, they note that Therminol would have the least pumping losses (however, no values are given) and that this parameter should also be included in a comparison. The authors also include the storage material cost of the HTF in their analysis with the Solar Salt system being the cheapest one. Furthermore, they perform a parametric study on the height-to-diameter ratio of the tank resulting in an increased efficiency for higher ratios.

Reddy et al. [18] perform a comparison between Therminol VP-1, Solar Salt and HITEC in a packed bed storage with a capacity of $40\,MWh_{th}$. The temperature range is adapted to a parabolic trough plant (300 °C to 410 °C). The storage efficiency chosen for the comparison is the ratio of energy extracted during discharge to the energy delivered in an ideal charge. They compare the efficiencies of the different HTFs while keeping the tank diameter and height constant, resulting in highest efficiencies for

Therminol VP-1, followed by Solar Salt and HITEC. Furthermore, they conduct a parametric study regarding the bed porosity and conclude that a porosity in the range of 0.15 to 0.35 is desirable. The authors also state that with very low porosities the pumping power is not negligible anymore, however, no values are given.

The literature review on comparative papers shows disagreement concerning the storage parameters that are kept constant and the definition of the efficiency. Furthermore, the storage costs and the pumping power required are typically not included in these papers. Moreover, no comparison of high temperature fluids for an advanced power cycle, including any liquid metals, has been conducted yet. These gaps shall be filled with this paper.

3. Methodology

The methodology for the comparison of sodium and high temperature salts in the thermocline packed bed is explained in this section. The reference case for the comparison (Section 3.1), the storage parameters (Section 3.2), the selected performance parameters (Section 3.3) and the definition of the storage cost for the economic analysis are introduced (Section 3.4). Finally, the selection of parameters for the parameteric study and the range they are varied in are presented (Section 3.5).

3.1. Reference case

The comparison in our work is based on a packed bed storage with a capacity similar to the one chosen by Reddy et al. [18]. It is applied to operating temperatures suitable for an advanced power cycle with an electric output of $4\,\mathrm{MW_e}$. With an assumed efficiency of 40 % in the power block, a thermal power of $10\,\mathrm{MW_{th}}$ is necessary from the storage system during discharge. With a discharge time of $4\,\mathrm{h}$ this leads to a necessary thermal storage capacity of $40\,\mathrm{MWh_{th}}$. This storage capacity is kept constant throughout the paper, while the dimensions of the tank are calculated depending on the physical properties of each HTF (see Section 3.2). Furthermore, the bed porosity, the tank diameter-to-height ratio, the filler material and diameter are defined and listed below (comparable to the experiment of Pacheco et al. [12]).

- Discharge time: $\Delta t = 4\,\mathrm{h}$
- Storage capacity: $Q = 40\,\mathrm{MWh_{th}} = 144\,\mathrm{GJ_{th}}$
- $T_{\min} = 500\,^{\circ}\mathrm{C}$, $T_{\max} = 700\,^{\circ}\mathrm{C}$
- Porosity: $\varepsilon = 0.22$
- Tank diameter-to-height ratio: $D/H = 0.5$
- Filler material: Quartzite ($\mathrm{SiO_2}$)
- Filler diameter: $d = 0.015\,\mathrm{m}$

3.2. Storage parameters

With the previously defined reference case, the resulting storage tank height (H), mass flow rate ($\dot{m}$), liquid quantity (m_f) and solid quantity (m_s) can be calculated

for each HTF depending on the fluid and solid properties (Table 1).

$$H = \left(\frac{4Q}{\pi (D/H)^2 (\rho_\mathrm{f} c_{pf}\varepsilon + \rho_\mathrm{s} c_{ps}(1-\varepsilon))\,(T_{\max} - T_{\min})} \right)^{1/3}$$ (1)

$$m_\mathrm{f} = \frac{\varepsilon \rho_\mathrm{f} Q}{(\rho_\mathrm{f} c_{pf}\varepsilon + \rho_\mathrm{s} c_{ps}(1-\varepsilon))\,(T_{\max} - T_{\min})}$$ (2)

$$m_\mathrm{s} = \frac{(1-\varepsilon)\rho_\mathrm{s} Q}{(\rho_\mathrm{f} c_{pf}\varepsilon + \rho_\mathrm{s} c_{ps}(1-\varepsilon))\,(T_{\max} - T_{\min})}$$ (3)

$$\dot{m} = \frac{Q}{c_{pf}\Delta t\,(T_{\max} - T_{\min})}$$ (4)

Table 1: Physical properties at $T_{\max} = 700\,^{\circ}\mathrm{C}$, HTS 1 := ZnCl$_2$-NaCl-KCl, HTS 2 := MgCl$_2$-KCl and HTS 3 := Na$_2CO_3$-K$_2CO_3$-Li$_2CO_3$

	c_p	ρ	λ	μ	Ref.
	Jkg⁻¹K⁻¹	kg m⁻³	Wm⁻¹K⁻¹	mPas	
Na	1256	798	57.5	0.2	[19]
HTS 1	900	1977	0.29	4.2	[20]
HTS 2	1150	1660	0.5	5.0	[8],[21]
HTS 3	1612	1848	0.47	5.9	[22]
SiO$_2$	1050	2640	2.5	-	[23]

3.3. Performance parameters

In this subsection three performance parameters are defined: the discharge efficiency, the standby efficiency and the pumping power.

In the literature, several definitions of the efficiency of a packed bed storage are proposed (see Section 2). Haller et al. [24] gives an overview of definitions of those efficiencies. In this paper, the definition in Equation 5 is used. It is the ratio of extracted energy during discharge $Q_\mathrm{dis,out}$ compared to the initial sensible heat $Q_\mathrm{chg,in,max}$ in an ideal charging step. The discharge mass flow $\dot{m}$ is assumed to be the same as the charge mass flow, and the discharge time t_dis the same as the charge time t_chg. This definition allows a direct comparison to a two tank arrangement, which would have an efficiency of 100 % assuming perfect insulation. It implies that all the outgoing thermal energy can be used regardless of which temperature. As this work aims to primarily compare different HTFs, this definition is sufficient.

$$\eta = \frac{Q_\mathrm{dis,out}}{Q_\mathrm{chg,in,max}} = \frac{\int_0^{t_\mathrm{dis}} \dot{m}(c_{pf}T_\mathrm{f,dis,out}(t) - c_{pf}T_{\min})\,\mathrm{d}t}{\int_0^{t_\mathrm{chg}} \dot{m}(c_{pf}T_{\max} - c_{pf}T_{\min})\,\mathrm{d}t}$$ (5)

The standby efficiency is evaluated using the thickness of the thermocline region Δx_tc, which increases over the standby time t_standby, related to the height of the tank

H (Equation 6). The limits of the thermocline region are defined by $T_{\min}$ + 5 K and $T_{\max}$ - 5 K, similar to Ref. [25].

$$\zeta = \frac{\Delta x_{\text{tc}}(t_{\text{standby}})}{H} \tag{6}$$

The pumping power is evaluated according to Equation 7 with the pressure loss calculated with the Ergun equation (Equation 8) using the velocity u_0 through the cross-sectional area of an empty tank (Equation 9) [26].

$$P = \dot{V}\Delta p = \frac{\dot{m}}{\rho_{\text{f}}}\Delta p \tag{7}$$

$$\frac{\Delta p}{H} = 150\frac{(1-\varepsilon)^2}{\varepsilon^3}\frac{\mu_{\text{f}}u_0}{d^2} + 1.75\frac{(1-\varepsilon)}{\varepsilon^3}\frac{\rho_{\text{f}}u_0^2}{d} \tag{8}$$

$$u_0 = \frac{4\dot{m}}{\rho_{\text{f}}\pi(D/H)^2H^2} \tag{9}$$

3.4. Material cost

Bulk storage material costs alone are considered in this economic comparison, independent of the additional costs associated with the tanks and balance-of-system components. It is assumed that for an equivalent capacity storage system, these additional costs are of similar magnitude. The overall storage material cost related to the energy content of a packed bed thermal energy storage (M) is calculated with Equation 10 based on the material cost data of the fluid (C_{f}) and the filler material (C_{s}), which are listed in Table 2. The costs data of the molten salts are adjusted to the currency of December 2016 using the producer price index commodity data for industrial chemicals provided by the Bureau of Labour Statistics [27].

$$M = \frac{\varepsilon\rho_{\text{f}}C_{\text{f}} + (1-\varepsilon)\rho_{\text{s}}C_{\text{s}}}{(\varepsilon\rho_{\text{f}}c_{p\text{f}} + (1-\varepsilon)\rho_{\text{s}}c_{p\text{s}})(T_{\max} - T_{\min})} \tag{10}$$

Table 2: Material cost data of fluids and filler, HTS 1 := ZnCl$_2$-NaCl-KCl, HTS 2 := MgCl$_2$-KCl and HTS 3 := Na$_2$CO$_3$-K$_2$CO$_3$-Li$_2$CO$_3$

	Na	HTS 1	HTS 2	HTS 3	SiO$_2$
C (€kg^{-1})	2.6	1.3	0.4	2.6	0.5
Ref.	[28]	[29],[30]	[30],[31]	[30],[32]	[28]

3.5. Parametric study

The effects of the porosity (ε), the tank diameter-to-height ratio (D/H) and the particle diameter (d) on the discharge efficiency (η), pumping power (P), storage cost (M) and thermocline thickness (ζ) during standby are studied. Table 3 shows which storage parameter has an impact on which performance parameter, marked by a tick. For each parameter, the storage capacity is kept constant as previously defined in the reference case (Section 3.1) and the storage parameters are calculated according to the equations given in Section 3.2.

Table 3: Varied parameters, their range and the affected performance parameters

Parameter	Range	η	P	M	ζ
ε	[0.1,0.22,0.5,0.7,0.9]	✓	✓	✓	✓
D/H	[0.2,0.5,1.0,1.5]	✓	✓	-	✓
d (mm)	[5,15,30,50]	✓	✓	-	-

4. Model description

The temperature distributions of the fluid (HTF) and solid material (filler) are mathematically described by a one-dimensional two-phase model as described in Ref. [33]. For this comparison the velocity and the inlet temperature are taken as uniform over the cross-section of the tank. This is typically achieved by using a distributor. Moreover, the porosity is assumed to be uniformly distributed and the wall of the tank is considered to be perfectly insulated. With these assumptions the temperature distribution varies only along the tank axis and thus a one-dimensional mathematical model can be used. The validity of this approach is confirmed in Section 4.6 by comparison with existing experimental data.

For molten salts, a lumped capacitance can be assumed for the solid phase leading to a simplified model. However, in a sodium thermocline storage with filler material, the internal heat diffusion in the filler particles has to be considered due to significantly higher Biot numbers.

The Biot-number is defined by Bi = $\alpha \cdot (d/2)/\lambda_{\text{s}}$ with the heat transfer coefficient α = Nu $\cdot \lambda_{\text{f}}/d$. The filler particles are modelled as spheres of diameter d. As the flow in the packed bed is very slow, a minimum Nusselt number Nu = 2 (only conduction) is assumed as a conservative estimation. In this case, the definition of the Biot number simplifies to Bi = $\lambda_{\text{f}}/\lambda_{\text{s}}$. This results in Bi $\approx$ 0.1 for the molten salts and Bi $\approx$ 11.6 for molten sodium, according to the properties of Table 1.

In contrast to molten salt, the Biot number of the sodium system is $\gg$ 1 and therefore the assumption of a uniform temperature distribution within the solid is not valid anymore [34]. Thus, the diffusion process inside the solid spheres needs to be considered.

A simplified model (Section 4.1) can therefore only be applied for molten salts (see Figure 1 left). For liquid sodium, a model including heat diffusion in the filler particles is used (see Figure 1 right). The energy equations solved for both models are presented in the following.

4.1. Model I: Molten salts

The temperature distribution in a molten salt thermocline storage with filler is calculated with a one-dimensional two-phase model with the assumption of a simplified lumped capacitance for the solid phase due to low Biot numbers $\ll$ 1. The energy equation for the fluid phase is given in Equation 11 and for the solid phase in Equation 12.

4
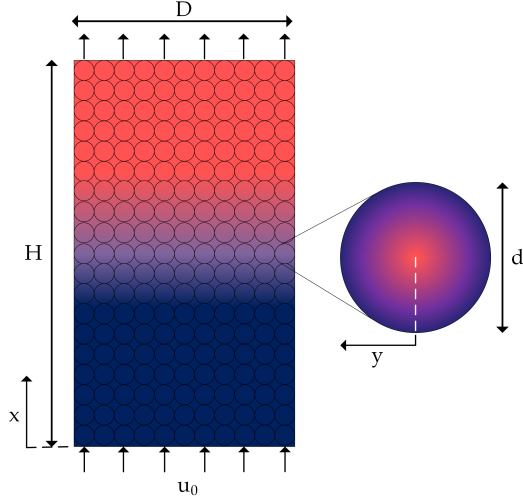
Figure 1: Left: schematic temperature distribution in storage tank during discharge; Right: schematic temperature distribution in filler particle during discharge

The equations are coupled by the volumetric heat transfer coefficient h_v in a source/sink term.

$$\varepsilon \rho_\mathrm{f} c_{pf} \left(\frac{\partial T}{\partial t} + u \frac{\partial T}{\partial x} \right) = \varepsilon \lambda_\mathrm{f} \frac{\partial^2 T}{\partial x^2} - h_\mathrm{v}(T - T_s) \tag{11}$$

$$(1 - \varepsilon) \rho_\mathrm{s} c_{ps} \frac{\partial T_\mathrm{s}}{\partial t} = h_\mathrm{v}(T - T_s) \tag{12}$$

4.2. Model II: Sodium

The temperature distribution for liquid sodium is also determined with a one-dimensional two-phase model, however, the intra-particle diffusion is considered specifically. The energy equation for the fluid phase is given in Equation 13 and for one representative filler particle in Equation 14. The filler particles are assumed to be spheres in this model. The equations are coupled by the last term in Equation 13 being it also the boundary condition at the surface of the filler spheres (Equation 19).

$$\varepsilon \rho_\mathrm{f} c_{pf} \left(\frac{\partial T}{\partial t} + u \frac{\partial T}{\partial x} \right) = \varepsilon \lambda_\mathrm{f} \frac{\partial^2 T}{\partial x^2} - h_\mathrm{v}(T - T_\mathrm{p}\big|_{y=\frac{d}{2}}) \tag{13}$$

$$\rho_\mathrm{s} c_{ps} \frac{\partial T_\mathrm{p}}{\partial t} = \lambda_\mathrm{s} \left(\frac{\partial^2 T_\mathrm{p}}{\partial y^2} + \frac{2}{y} \frac{\partial T_\mathrm{p}}{\partial y} \right) \tag{14}$$

In both models, the axial diffusion in the solid phase is neglected because point contact between the spherical filler particles is assumed. Furthermore, the tank is ideally insulated and thus heat losses to the ambient are neglected. A uniform velocity and temperature are assumed at the inlet of the packed bed, which can be realized by well-designed distributors. Temperature dependent properties for the HTFs and constant properties for the solid filler material are used, according to references listed in Table 1.

4.3. Initial and boundary conditions

The initial condition at $\mathrm{t} = 0$ is a homogeneous constant temperature in the tank. This temperature is either T_max (fully charged) or T_min (fully discharged). If several cycles are considered, a temperature distribution in the tank is applied as the initial condition for the next step.

$$t = 0: \quad \begin{cases} T(x) = T_\mathrm{s}(x) = T_\mathrm{p}(x,y) = T_\mathrm{max} \\ T(x) = T_\mathrm{s}(x) = T_\mathrm{p}(x,y) = T_\mathrm{min} \\ T(x) = f(x), T_\mathrm{s}(x) = g(x), T_\mathrm{p}(x,y) = h(x,y) \end{cases} \tag{15}$$

As boundary condition for the fluid, constant temperature at the inlet ($x = 0$) and zero heat flux at the outlet of the tank ($x = H$) are imposed. It is assumed that the solid material does not exchange energy at the inlet and outlet of the tank.

$$x = 0: \qquad T = T_{in} \qquad \frac{\partial T_s}{\partial x} = 0 \tag{16}$$

$$x = H: \qquad \frac{\partial T}{\partial x} = 0 \qquad \frac{\partial T_s}{\partial x} = 0 \tag{17}$$

In the core of the solid particles ($y = 0$) a symmetry condition is applied. At the surface ($y = \mathrm{d}/2$) heat is exchanged with the fluid, which is taken into account by a convection boundary condition.

$$y = 0: \qquad \frac{\partial T_\mathrm{p}}{\partial y} = 0 \tag{18}$$

$$y = d/2: \qquad -\lambda_s \frac{\partial T_\mathrm{p}}{\partial y} = h_\mathrm{v}(T - T_p) \tag{19}$$

4.4. Heat transfer between fluid and filler

The volumetric heat transfer coefficient h_v is linked to the (surface specific) heat transfer coefficient α by the specific surface of the particles in the bed. The heat transfer coefficient α between fluid and filler is being calculated with Nusselt correlations for a packed bed.

$$h_\mathrm{v} = \alpha \frac{6(1 - \varepsilon)}{d} \qquad \alpha = \frac{\mathrm{Nu}_\mathrm{bed} \cdot \lambda_\mathrm{f}}{d} \tag{20}$$

The Nusselt correlation of Wakao and Kaguei [35] is widely used for molten salts in the literature, although it is valid for gases ($\mathrm{Pr} \approx 0.7$).

$$\mathrm{Nu} = 2 + 1.1 \mathrm{Re}_\mathrm{p}^{0.6} \mathrm{Pr}^{1/3} \qquad 15 \leq \mathrm{Re}_\mathrm{p} \leq 8500 \tag{21}$$

For sodium or liquid metals in general, which have a significantly low Prandtl numbers, no packed bed heat transfer correlation can be found in the literature. There is a correlation of Melissari and Argyropolus [36] for a wide range of Prandtl numbers ($0.003 < \mathrm{Pr} < 10$).

$$\mathrm{Nu} = 2 + 0.47 \mathrm{Re}_\mathrm{p}^{0.5} \mathrm{Pr}^{0.36} \qquad 10^2 \leq \mathrm{Re}_\mathrm{p} \leq 5 \cdot 10^4 \tag{22}$$

However, this correlation is derived from experimental data for a single sphere and not for a packed bed. Therefore, only conductive heat transfer is assumed as conservative assumption for the simulations with sodium in this study, which leads to the minimum Nusselt number for a sphere of $\mathrm{Nu} = 2$.

4.5. Solution procedure

The equations are solved with a finite volume method that has been implemented in MATLAB®. The second-order Crank-Nicolson scheme is used for the time discretization. A central difference scheme and a first order upwind scheme are used for the spatial discretization of diffusive and advective terms, respectively.

A sensitivity analysis for the number of control volumes (CVs) in the tank and in the filler particles has been conducted for all configurations presented in this paper. The number of CVs is defined as satisfactory if the outlet temperature differs less than 0.1 % from that of the next finest grid.

A cycle is considered to be stable if the temperature at the end of a discharge step of two subsequent cycles differs no more than 0.1 %.

4.6. Validation with experimental data

The code is validated with experimental data from a molten salt experiment (2.3 MWh$_{th}$) by Sandia National Laboratories [12]. The temperature distribution at t = 0 is fitted and taken as initial condition for the simulation of a 2 h discharging process. The thermo-physical properties of Solar Salt and the filler material quartzite (rocks and sand) are assumed constant in the considered temperature range and are taken from Ref. [23]. The experimental and simulated fluid temperature distributions at the beginning of the discharge and after 0.5 h, 1 h, 1.5 h and 2 h are shown in Figure 2. The experimental and simulation data are in quite good agreement.
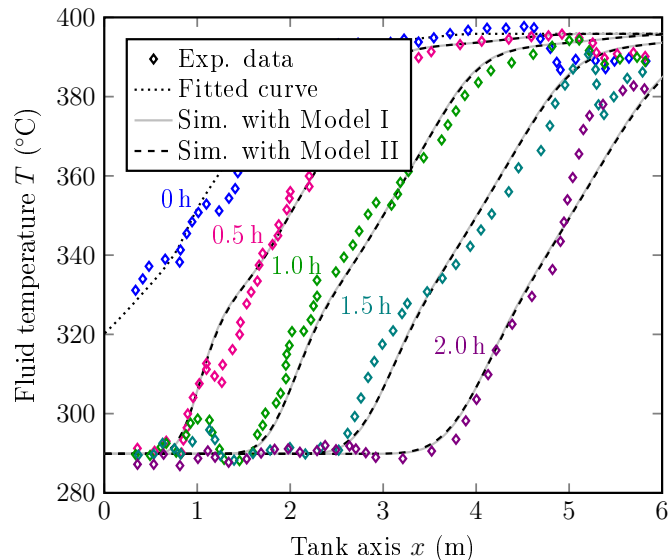
Figure 2: Validation with experimental data from Sandia Laboratories experiment (taken from Ref. [12]), Model I: 500 CVs in tank axis, time step = 3.6 s, Model II: 500 CVs in tank axis, 50 CVs in particle, time step = 3.6 s

A second validation is conducted using data from the Solar One storage test (170 MWh$_{th}$) with thermal oil as HTF and granite rock and sand as filler material [11].

Again, the temperature distribution at t = 0 is fitted and taken as initial condition for the simulation of a 8 h discharging process. The fluid properties of thermal oil (Caloria HT) are taken from Ref. [37] and the solid properties from Ref. [38]. Again, the experimental and numerical results shown in Figure 3 are in good agreement after 4 h and 8 h discharge time.
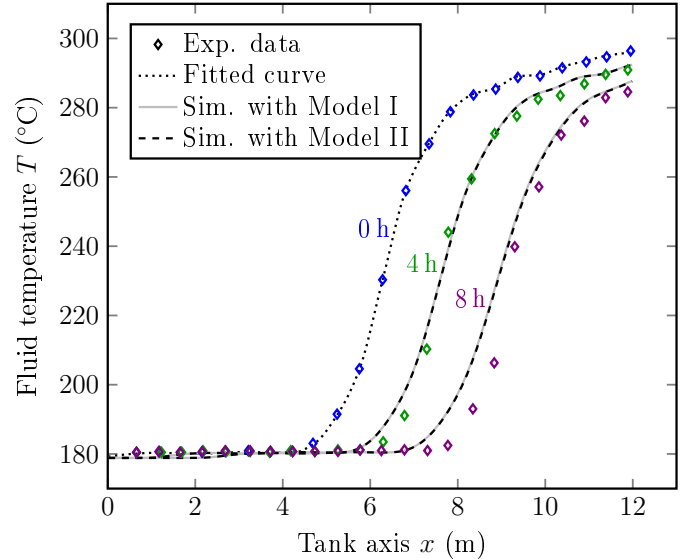
Figure 3: Validation with experimental data from Solar One (taken from Ref. [38]), Model I: 500 CVs in tank axis, time step = 7.2 s, Model II: 500 CVs in tank axis, 30 CVs in particle, time step = 7.2 s

The average difference between the numerically calculated (T_{num}) from the experimental temperatures (T_{exp}) is ≈ 4 K and the relative mean square error is $< 1.6\,10^{-4}$ (calculated from $1/n \sum ((T_{exp} - T_{num})/T_{exp})^2$). These figures are in the same range as those obtained by Hoffmann et al. [38] comparing results from a one-dimensional two-phase model without heat losses with their experimental values.

It has to be noted that packed bed porosities smaller than 0.26 (closest packing of spheres) can only be achieved with non-uniformly sized filler spheres [39]. However, we assume uniformly sized filler spheres in our model. The validation cases both have porosities of 0.22 and are thus below this limit. Nevertheless, the validation using this value with uniformly sized filler material has been satisfactory. Therefore, we also use this porosity with uniformly sized filler particles for our reference case despite being below the limit of 0.26.

4.7. Thermocline degradation

During standby only heat conduction is present and the thermal conductivity of the filler material cannot be neglected anymore. A homogenous model is used where only molecular diffusion of energy is considered by an effective "mixed" thermal diffusivity accounting for both solid and

liquid phase, resulting in the following equation:

$$\frac{\partial T_{\mathrm{mix}}}{\partial t} = a_{\mathrm{mix}} \frac{\partial^2 T_{\mathrm{mix}}}{\partial x^2} \tag{23}$$

The mixed thermal diffusivity of the homogenous phase is defined according to Ref. [25]:

$$a_{\mathrm{mix}} = \frac{\varepsilon \lambda_{\mathrm{f}} + (1 - \varepsilon)\lambda_{\mathrm{s}}}{\varepsilon \rho_{\mathrm{f}} c_{pf} + (1 - \varepsilon)\rho_{\mathrm{s}} c_{ps}} \tag{24}$$

An ideal thermocline is assumed as initial condition for the assessment of the standby behaviour, i.e. the bottom half of the tank is at the minimum temperature, whereas the upper half is at the maximum temperature.

$$t = 0: \quad \begin{cases} T_{\mathrm{mix}}(x) = T_{\mathrm{min}} & 0 \leq x \leq H/2 \\ T_{\mathrm{mix}}(x) = T_{\mathrm{max}} & H/2 < x \leq H \end{cases} \tag{25}$$

As boundary conditions, no heat exchange is assumed at the top and bottom of the tank.

$$x = 0 \wedge H: \quad \frac{\partial T_{\mathrm{mix}}}{\partial x} = 0 \tag{26}$$

5. Results

Initially, the storage tank is fully charged with fluid and filler being at maximum temperature (T_{max}) and then discharged for 4 h. After that, the storage is charged again for 4 h. This is repeated until a stable cycle is reached.

5.1. Reference case

The parameters that define the reference case are listed in Section 3.1. Based on the different physical properties of the fluids, the resulting storage parameters are displayed in Table 4. In the following, the molten salts are abbreviated with HTS 1 (ZnCl$_2$-NaCl-KCl), HTS 2 (MgCl$_2$-KCl) and HTS 3 (Na$_2$CO$_3$-K$_2$CO$_3$-Li$_2$CO$_3$).

Table 4: Storage and simulation parameters for reference case with physical properties at T_{max}, HTS 1 := ZnCl$_2$-NaCl-KCl, HTS 2 := MgCl$_2$-KCl and HTS 3 := Na$_2$CO$_3$-K$_2$CO$_3$-Li$_2$CO$_3$

	Na	HTS 1	HTS 2	HTS 3
Height H (m)	11.5	11.3	11.2	10.9
Fluid mass m_{f} (tons)	53	123	102	104
Solid mass m_{s} (tons)	622	581	574	526
Mass flow $\dot{m}$ (kg s^{-1})	39.8	55.6	43.5	31.0
Velocity u_0 (mm s^{-1})	1.9	1.1	1.1	0.7
Pumping power P (W)	22	64	64	31
Cost M (€kW^{-1}h^{-1})	11.2	11.2	8.2	13.3
Model	II	I	I	I
CVs in tank axis	1000	500	500	500
CVs in particle	70	-	-	-
Time step (s)	2.9	4.8	4.8	4.8

The storage tank with sodium is the largest one due to

its lowest volumetric thermal capacity ($\rho_{\mathrm{f}} c_{pf}$) compared to the salts. However, the fluid mass of sodium is lowest due to its lower density compared to the salts. Furthermore, sodium requires the least pumping power compared to the salts due to its low viscosity (Equation 8). However, it has to be noted, that all pumping power figures are very low due to the low fluid velocities in the tank.

The packed bed storage with HTS 2 is the least expensive one due to the very low-cost of the chloride salts. It would be even cheaper without the chosen filler material (6.3 €/kWh). Nevertheless, HTS 2 is also included in this study, as cost reduction is possible in principle, if other cheaper filler materials are chosen.
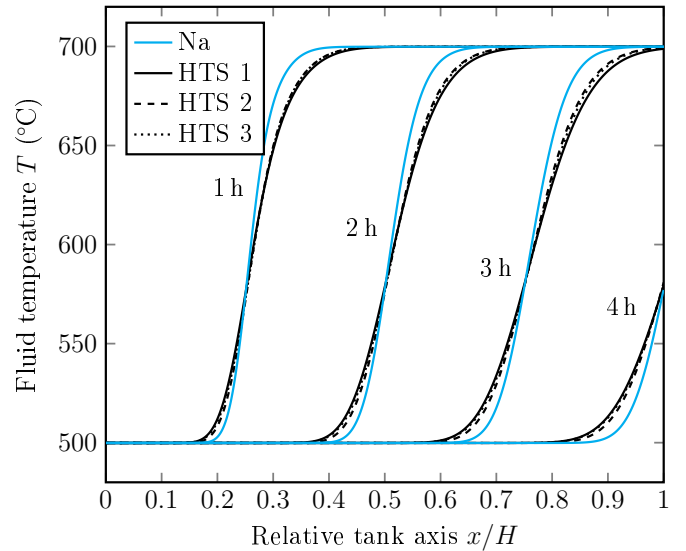
Figure 4: Temperature distributions of Na and salts during discharge in the stable (fourth) cycle starting from a fully charged tank in the first cycle
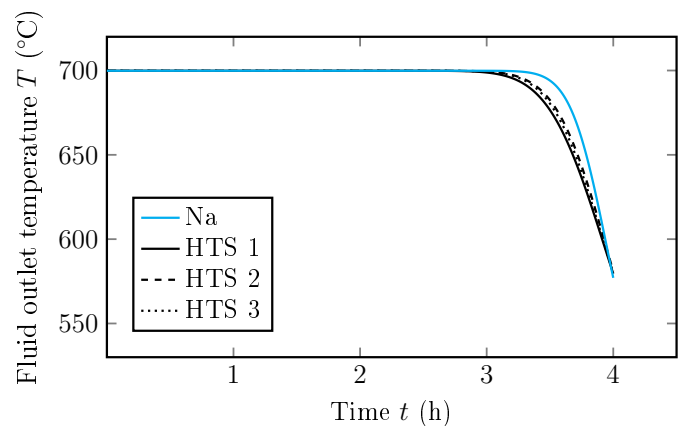
Figure 5: Fluid outlet temperature of Na and salts discharge in the stable (fourth) cycle starting from a fully charged tank in the first cycle

The temperature distributions during discharging in a stable cycle along the tank axis at time intervals of 1 h are shown in Figure 4. The corresponding outlet temper-

7

atures (at $x = H$) over the discharge time are displayed in Figure 5. In the case of sodium, energy can be extracted from the storage at the maximum temperature for a longer period of time than for HTS 2, followed by HTS 3 and HTS 1. This leads to discharge efficiencies of 97.8 % (Na), 97.2 % (HTS 2), 97.0 % (HTS 3) and 96.7 % (HTS 1) in the first cycle. The efficiencies decrease to 96.8 % (Na), 95.7 % (HTS 2), 95.5 % (HTS 3) and 95.2 % (HTS 1) in a stable cycle (Figure 6). A stable cycle is reached after three cycles for all considered fluids.
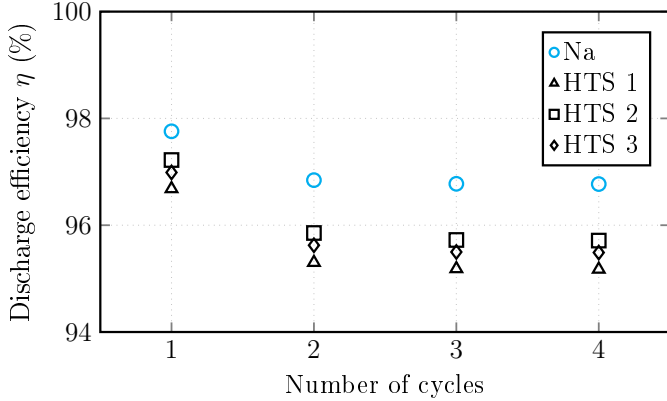
Figure 6: Discharge efficiencies vs. number of cycles

The slightly higher discharge efficiency of sodium compared to the salts is due to its higher heat transfer coefficient (Table 5) resulting from its significantly higher thermal conductivity compared to that of the considered salts ($\approx$ 100 times higher). Therefore, the thermal energy can be transferred into the filler faster leading to steeper fluid temperature gradients along the tank axis (see Figure 4). Due to the lack of suitable Nusselt correlations for a packed bed for low Prandtl number fluids, a constant value of Nu = 2 is assumed. Thus, the heat transfer coefficient (and thereby the discharge efficiency) is even underestimated here. In Table 5, the values resulting from the correlation of Melissari and Argyropoulos (Equation 22) are given in brackets, resulting in practically the same discharge efficiency. Among the molten salts, the best efficiencies are also reached for the highest heat transfer coefficients.

Table 5: Heat transfer characteristics at $T_{\max}$, *with Equation 22, HTS 1 := ZnCl$_2$-NaCl-KCl, HTS 2 := MgCl$_2$-KCl and HTS 3 := Na$_2$CO$_3$-K$_2$CO$_3$-Li$_2$CO$_3$

	Na	HTS 1	HTS 2	HTS 3
Nu	2 (2.7*)	11.3	8.7	8.2
h_v (kWm^{-3}K^{-1})	2392 (3251*)	66	91	80
η (%)	96.8 (96.9*)	95.2	95.7	95.5

However, a high thermal conductivity is disadvantageous if standby periods are considered between charging and discharging. Figure 7 shows the temperature distribution along the tank height (11 m) after 12 h, 24 h and 4 days of standby for sodium and HTS 1.
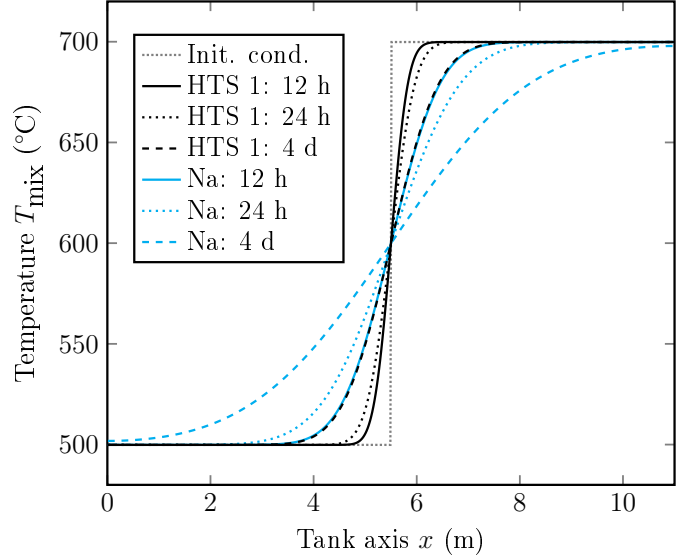
Figure 7: Standby behaviour of a packed bed with Na and HTS 1 after 12 h, 24 h and 4 days

Starting from an ideal step function, the thermocline region expands much faster for a sodium packed bed system than for one with salts. This is due to the one order of magnitude larger effective thermal diffusivity a_{mix} of the sodium packed bed system compared to the salt cases (see Table 6).

Table 6: Thermal diffusivity for standby simulation at $T_{\max}$, HTS 1 := ZnCl$_2$-NaCl-KCl, HTS 2 := MgCl$_2$-KCl and HTS 3 := Na$_2$CO$_3$-K$_2$CO$_3$-Li$_2$CO$_3$

	Na	HTS 1	HTS 2	HTS 3
a_{mix} (m^{2}s^{-1})	6.6 10^{-6}	7.8 10^{-7}	8.0 10^{-7}	7.2 10^{-7}
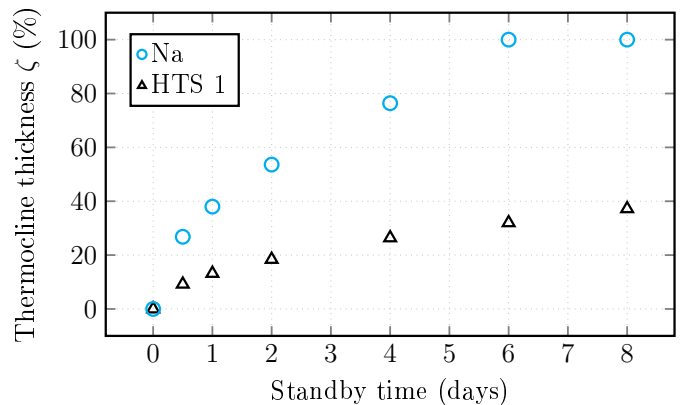
Figure 8: Thermocline thickness vs. standby time

The three salts show no noticeable difference in the temperature distribution, as the mixed thermal diffusivities are of the same order of magnitude. Therefore, only HTS 1

8

is displayed here as a representative salt. The thermocline thickness reaches 100 % of the tank height for a sodium packed bed system after 6 days, whereas the thermocline of the salt packed bed system takes up only 32 % in the same period (Figure 8). Even after 12 h of standby, the thermocline expands to more than 25 % of the tank for the sodium system compared to 10 % for HTS 1.

It can be concluded that a sodium packed bed system has higher efficiencies during cycling due to high heat transfer coefficients, resulting in sharp temperature gradients along the tank axis. However, these latter temperature gradients cannot be maintained over long standby periods between cycling. In case of the considered molten salts the opposite conclusions can be drawn.

5.2. Parametric study

In the parametric study, the effect of the porosity, the tank diameter-to-height ratio and the particle diameter on the discharge efficiency (after reaching a stable cycle), pumping power, storage cost and thermocline degradation during a certain standby period are investigated. For each investigated parameter the remaining parameters (including the storage capacity) are kept constant as defined in the reference case (Section 3.1).

Firstly, the porosity (ε) is varied from 0.1 to 0.9. Changing ε leads to different tank dimensions. All four considered performance parameters are influenced by ε (Table 3). For molten salts, the discharge efficiency (in a stable cycle) increases with increasing ε, i.e. increasing fluid volume fraction (Figure 9a). However, for molten sodium, it is the opposite: the discharge efficiency increases with decreasing ε, i.e. increasing solid volume. Sodium shows best efficiencies for low ε, because this leads to the lowest thermal conductivity in the packed bed ($\varepsilon\lambda_\mathrm{f}$), implying a steeper temperature profile. At the same time, the volumetric heat transfer coefficient (h_v) remains high enough to guarantee a very good energy exchange between fluid and filler material (Table 7). In contrast, the thermal conductivity of molten salts is very low at all ε, but the bottleneck are the low values of h_v, implying a quite ineffective heat transfer to the filler material. Therefore, a high amount of fluid, and thus high ε, are advantageous. It has to be noted that a validity range of the correlation of Wakao and Kaguei (Section 4.4) with respect to the porosity is not given in Ref. [35]. For low values of porosity, $\varepsilon = 0.22$, the validation with experimental data (Figures 2 and 3) shows the validity of the correlation. However, for high porosity values, $\varepsilon = 0.7$ and 0.9, the correlation must be used with caution because of the lack of experimental data for a validation.

To illustrate the impact of ε on the thermocline thickness, the latter is evaluated after 4 days standby starting from an ideal step function (Figure 9b). It has to be noted that varying ε not only influences the thermal diffusivity (a_mix), but also leads to a different tank height (due to keeping the storage capacity constant), which also influences the
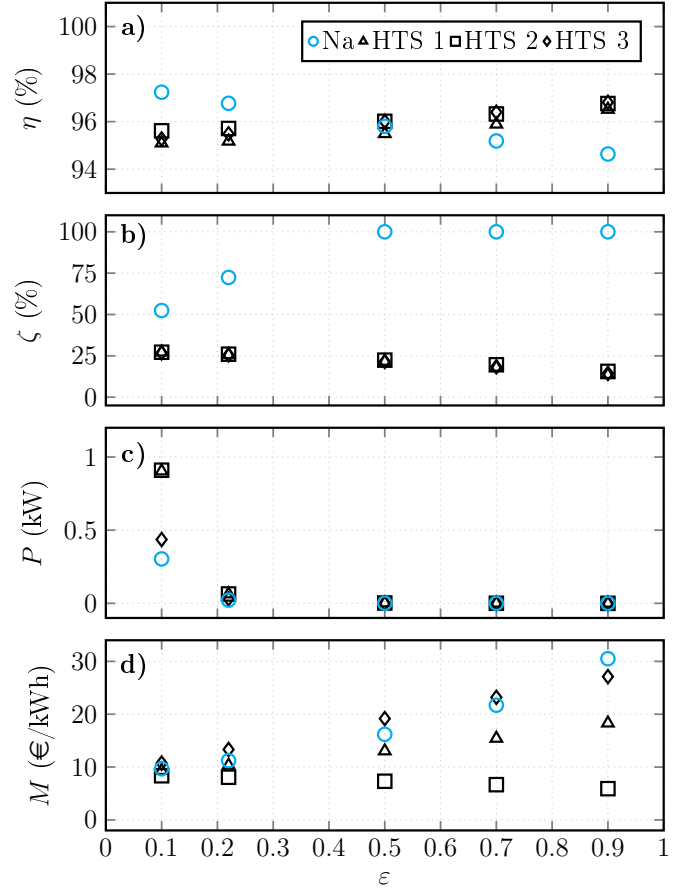
Figure 9: a) Discharge efficiency η (stable cycle) vs. porosity ε; b) Thermocline thickness ζ after 4 days vs. ε; c) Pumping power P vs. ε; d) Storage material cost M vs. ε

Table 7: Effect of porosity on thermal conductivity in the packed bed and volumetric heat transfer coefficient (at T_max), HTS 1 := ZnCl$_2$-NaCl-KCl

ε	Na		HTS 1	
	$\varepsilon\lambda_\mathrm{f}$	h_v	$\varepsilon\lambda_\mathrm{f}$	h_v
	Wm^{-1}K^{-1}	kWm^{-3}K^{-1}	Wm^{-1}K^{-1}	kWm^{-3}K^{-1}
0.10	5.8	2760	0.03	77
0.22	12.7	2392	0.06	66
0.50	28.8	1534	0.15	41
0.70	40.3	920	0.20	24
0.90	51.8	307	0.26	8

relative thermocline thickness during standby. For example, in the case of HTS 1 the height varies from 11.1 m ($\varepsilon = 0.10$) to 12.5 m ($\varepsilon = 0.90$), while for sodium from 11.2 m ($\varepsilon = 0.10$) to 14.6 m ($\varepsilon = 0.90$). The degradation of the thermocline (i.e. increasing thickness) intensifies for higher ε in the case of sodium due to the large thermal conductivity compared to the filler material. On the contrary, low values of ε lead to a higher degradation of the thermocline in case of molten salt, as the salt conductivity is lower than that of the filler.

9

The pumping power increases strongly for $\varepsilon < 0.22$ for all HTFs, with the lowest value required for sodium (Figure 9c). But even for ε of 0.1, the pumping power for all HTFs is lower than 0.03 % of the electric output of 4 MW. The storage cost decreases with decreasing porosity for HTS 1, HTS 2 and sodium due to lower cost of the filler material, however, for HTS 2 higher porosities are advantageous due to the lower cost of the fluid (Figure 9d).

The next parameter considered is the tank diameter-to-height ratio (D/H), which is varied from 0.2 to 1.5. The discharge efficiency (in a stable cycle) decreases with increasing D/H (Figure 10a). The effect is stronger for sodium than for the molten salts.
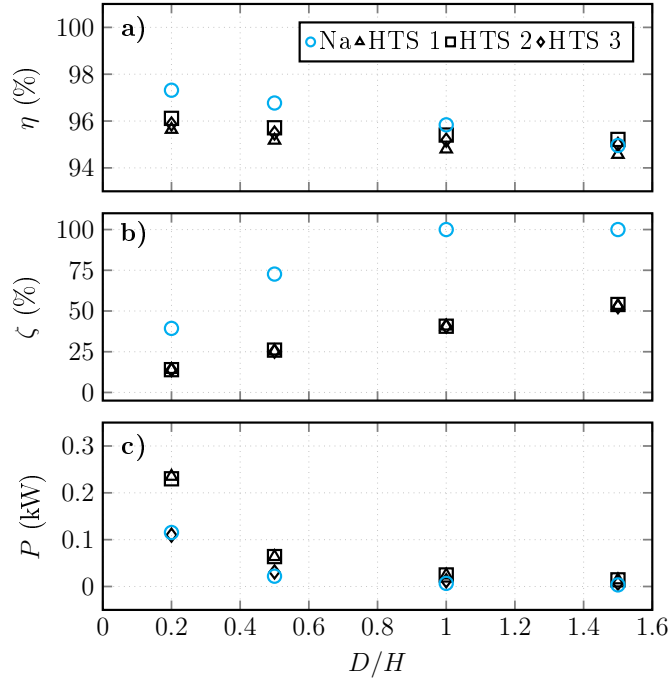
Figure 10: a) Discharge efficiency η (stable cycle) vs. diameter-to-height ratio D/H; b) Thermocline thickness ζ after 4 days vs. D/H; c) Pumping power P vs. D/H

Higher D/H mean larger tank diameters, which lead to lower fluid velocities. For salt, this implies also a decreasing heat transfer coefficient. In case of sodium, the minimum Nusselt number is assumed (Nu = 2) and therefore the velocity has no influence on the heat transfer coefficient used for the simulations. At the same time, higher D/H means smaller tank heights. Thus, the thermocline region accounts for a larger space compared to the total height. As the conductivity of sodium in the packed bed is much higher than for salt, this effect is more significant for sodium and explains the stronger influence of the D/H ratio on the discharge efficiency for sodium.

The effect of D/H on the standby behaviour is shown in Figure 10b. A smaller ratio is preferable, i.e. a high tank with a small diameter. For sodium the thermocline thickness after 4 days can be reduced from approximately 70 % ($D/H = 0.5$) to 40 % ($D/H = 0.2$) starting from an ideal

thermocline, and for salt from 25 % ($D/H = 0.5$) to 15 % ($D/H = 0.2$).

The D/H ratio also influences the pumping power. Lower D/H ratios, i.e. smaller tank diameters, lead to an increase in pumping power due to the higher velocity through the bed (Figure 10c).

The final parameter considered is the filler diameter (d), which is varied from 5 mm to 50 mm. Increasing the diameter of the filler material results in a decrease in discharge efficiency (in a stable cycle) for all HTFs (Figure 11a). A larger d leads to an increase of the Nusselt number due to an increasing Reynolds number (Re_p) for the molten salts (Equation 21). However, the heat transfer coefficient (α) and volumetric heat transfer coefficient (h_v) decrease with increasing diameter (Equation 20).
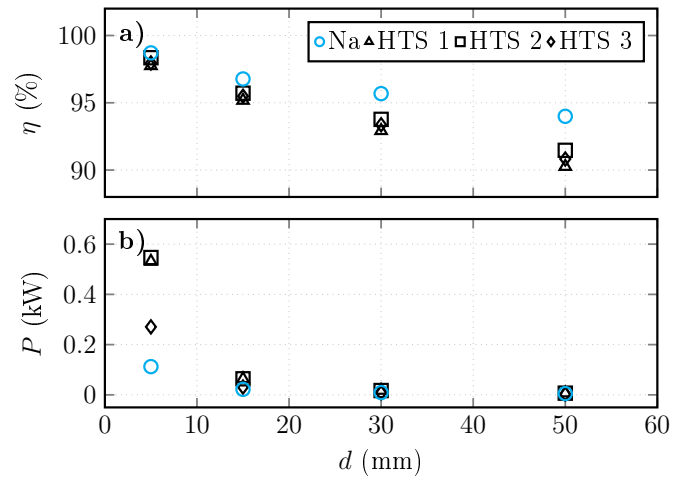
Figure 11: a) Discharge efficiency η (stable cycle) vs. filler diameter d; b) Pumping power P vs. d

Table 8: Effect of filler particle diameter on heat transfer from fluid to filler (at T_{max}), HTS 1 := ZnCl$_2$-NaCl-KCl

	d	Nu_{bed}	α	h_v
	mm	-	Wm^{-2}K^{-1}	kWm^{-3}K^{-1}
Na	5	2	23003	21531
	15	2	7668	2392
	30	2	3834	589
	50	2	2300	215
HTS 1	5	7	383	359
	15	11	211	66
	30	16	150	23
	50	21	118	11

In the case of sodium, a constant Nusselt number is assumed and therefore a decrease in d by a factor of 10 leads to a decrease in h_v by a factor of 100 (Table 8). For the molten salts, this effect is reduced due to the rising Nusselt numbers. Nevertheless, the decrease in discharge efficiency is still stronger for molten salt. This is due to the fact that the heat transfer is still excellent for large d in

case of sodium, but for molten salt, by contrast, it is much lower.

A reduced d results in an increase of the required pumping power (Figure 11b). However, this is still a small fraction (less than 0.02%) of the electric output of $4\,MW_e$ for all considered HTFs, even for the smalles considered diameter of $5\,mm$.

6. Conclusion

In this paper, the performance of sodium and three high temperature molten salts as HTFs in a packed bed thermal energy storage system is investigated. Quartzite spheres are taken as exemplary filler material neglecting chemical stability issues in the considered temperature range and compatibilty with the chosen fluids. A $40\,MWh_{th}$ storage system is numerically studied with a one-dimensional two-phase model. The discharge efficiency, pumping power, storage cost and thermocline degradation are analysed to assess the potential of this storage solution for future scientific investigations.

The packed bed system with sodium shows a slightly higher discharge efficiency (96.8%) than that obtained with molten salts (95.2 - 95.7%). The reason is the significantly higher thermal conductivity and therefore the higher heat transfer coefficient compared to molten salt. However, during standby the high effective thermal diffusivity of the sodium packed bed system leads to a faster expansion of the thermocline region. Furthermore, the required pumping power for sodium is lower than for the salts due to its lower viscosity. The storage material cost for sodium is $11.2\,€/kWh$, for the considered molten salts it ranges from $8.1\,€/kWh$ to $13.3\,€/kWh$.

In a parametric study, the influence of bed porosity, tank diameter-to-height ratio and filler size on the selected performance parameters is studied. To achieve high discharge efficiencies, a low tank diameter-to-height ratio and small filler diameters are preferable for all HTFs. Although still negligible in magnitude, more pumping power is needed in this case. In the case of sodium, the discharge efficiency can be further increased by decreasing the porosity in the bed (i.e. more filler). For molten salts, however, the discharge efficiency is higher for higher porosities (i.e. more HTF). The storage costs can also be minimized with low bed porosity, as the filler material is typically cheaper than the HTF (except for HTS 2). This leads to an efficient and economical storage system for sodium with a high amount of filler material, whereas an optimum between efficiency and investment cost needs to be found for the molten salts.

The standby behaviour for the sodium packed bed storage can be improved with low porosities and a small tank diameter-to-height ratio. For molten salts, a small tank diameter-to-height ratio is also preferable, however, in contrast to sodium, high porosities are beneficial due to a lower conductivity of the salts compared to the considered filler material.

All in all, sodium is slightly more efficient than the considered molten salt system during discharge, however, the high thermal conductivity leads to a fast degradation of the thermocline region during stand-by. Therefore, either only short standby times are allowed or the hotter part needs to be separated from the colder one during standby. This could be implemented by draining hot and cold sodium into separate tanks, using insulating layers or a multi-tank system. The molten salts, by contrast, are less-efficient HTFs in the packed bed storage, but have better standby behaviour.

Acknowledgement

Nomenclature

Subscripts

chg	Charge
dis	Discharge
f	Fluid
max	Maximum
min	Minimum
mix	Mixed
p	Particle
tc	Thermocline
s	Solid
v	Volumetric

Acronyms

CV	Control volume
HTF	Heat transfer fluid
HTS	High temperature salt
HTS 1	$ZnCl_2$-NaCl-KCl
HTS 2	$MgCl_2$-KCl
HTS 3	Na_2CO_3-K_2CO_3-Li_2CO_3

References

References

[1] S. Polimeni, M. Binotti, L. Moretti, G. Manzolini, Comparison of sodium and KCl-MgCl 2 as heat transfer fluids in CSP solar tower with sCO 2 power cycles, Solar Energy 162 (2018) 510–524.

[2] W. Stein, R. Buck, Advanced power cycles for concentrated solar power, Solar Energy 152 (2017) 91–105.

Latin letters

a	Thermal diffusivity [m^{2}s^{-1}]
C	Material cost [€kg^{-1}]
c_p	Heat capacity [Jkg^{-1}K^{-1}]
d	Filler particle diameter [m]
D	Tank diameter [m]
H	Tank height [m]
h_v	Volumetric heat transfer coefficient [Wm^{-3}K^{-1}]
m	Mass [kg]
M	Storage material cost [€kW^{-1}h^{-1}]
$\dot{m}$	Mass flow [kgs^{-1}]
Δp	Pressure difference [Pa]
P	Pumping power [W]
Q	Storage capacity [J]
t	Time [s]
T	Temperature [K]
u	Fluid velocity in packed bed $= u_0/\varepsilon$ [ms^{-1}]
u_0	Velocity through empty cross-sectional area [ms^{-1}]
$\dot{V}$	Volume flow [m^{3}s^{-1}]
Δx_tc	Thermocline thickness [m]
x	Coordinate along tank height
y	Coordinate along particle radius

Greek letters

α	Heat transfer coefficient [Wm^{-2}K^{-1}]
ε	Porosity [-]
ζ	Thermocline efficiency [–]
η	Discharge efficiency [-]
λ	Thermal conductivity [Wm^{-1}K^{-1}]
μ	Dynamic viscosity [Pas]
ρ	Density [kgm^{-3}]

Non-dimensional parameters

Bi	Biot number: $\mathrm{Bi} = \alpha \cdot (d/2)/\lambda_\mathrm{s}$
Nu	Nusselt number: $\mathrm{Nu} = \alpha \cdot d/\lambda_\mathrm{f}$
Pr	Prandlt number: $\mathrm{Pr} = \mu_\mathrm{f} \cdot c_{p\mathrm{f}}/\lambda_\mathrm{f}$
Re$_\mathrm{p}$	Reynolds number: $\mathrm{Re_p} = u_0 \cdot d \cdot \rho_\mathrm{f}/\mu_\mathrm{f}$

[3] J. Pacio, A. Fritsch, C. Singer, R. Uhlig, Liquid metals as efficient coolants for high-intensity point-focus receivers implications to the design and performance of next-generation CSP systems, Energy Procedia 49 (2014) 647 – 655. Proceedings of the SolarPACES 2013 International Conference.

[4] F. G. Casal, Solar thermal power plants : achievements and lessons learned exemplified by the SSPS Project in Almeria/Spain, Springer, 1987.

[5] J. Coventry, C. Andraka, J. Pye, M. Blanco, J. Fisher, A review of sodium receiver technologies for central receiver solar power plants, Solar Energy 122 (2015) 749–762.

[6] J. Pacio, C. Singer, T. Wetzel, R. Uhlig, Thermodynamic evaluation of liquid metals as heat transfer fluids in concentrated solar power plants, Applied Thermal Engineering 60 (2013) 295 – 302.

[7] K. Niedermeier, J. Flesch, L. Marocco, T. Wetzel, Assessment of thermal energy storage options in a sodium-based CSP plant, Applied Thermal Engineering 107 (2016) 386–397.

[8] M. Mehos, C. Turchi, J. Vidal, M. Wagner, Z. Ma, C. Ho, W. Kolb, C. Andraka, A. Kruizenga, Concentrating Solar Power Gen3 Demonstration Roadmap, Technical Report NREL/TP-5500-67464, National Renewable Energy Laboratory (NREL),

2017.

[9] B. Kelly, D. Kearney, Thermal Storage Commercial Plant Design Study for a 2-Tank Indirect Molten Salt System - Final report, Technical Report NREL/SR-550-40166, National Renewable Energy Laboratory, 2006.

[10] T. Esence, A. Bruch, S. Molina, B. Stutz, J.-F. Fourmigué, A review on experience feedback and numerical modeling of packed-bed thermal energy storage systems, Solar Energy 153 (2017) 628–654.

[11] G. J. Kolb, D. J. Alpert, C. W. Lopez, Insights from the operation of solar one and their implications for future central receiver plants, Solar Energy 47 (1991) 39 – 47.

[12] J. E. Pacheco, S. K. Showalter, W. J. Kolb, Development of a molten-salt thermocline thermal storage system for parabolic trough plants, J. Sol. Energy Eng. 124 (2002) 153.

[13] C. Odenthal, N. Breidenbach, T. Bauer, Modelling and operation strategies of DLR's large scale thermocline test facility (TESIS), AIP Conference Proceedings 1850 (2017) 080019.

[14] B. D. Pomeroy, Thermal energy storage in a packed bed of iron spheres with liquid sodium coolant, Solar Energy 23 (1979) 513–515.

[15] A. Modi, C. D. Perez-Segarra, Thermocline thermal storage systems for concentrated solar power plants: One-dimensional numerical model and comparative analysis, Solar Energy 100 (2014) 84–93.

[16] M. Cascetta, G. Cau, P. Puddu, F. Serra, Numerical investigation of a packed bed thermal energy storage system with different heat transfer fluids, Energy Procedia 45 (2014) 598–607.

[17] A. G. Vilella, S. Yesilyurt, Analysis of heat storage with a thermocline tank for concentrated solar plants: Application to AndaSol I, in: 2015 IEEE International Conference on Industrial Technology (ICIT), IEEE, 2015.

[18] K. Reddy, V. Jawahar, S. Sivakumar, T. Mallick, Performance investigation of single-tank thermocline storage systems for CSP plants, Solar Energy 144 (2017) 740–749.

[19] O. J. Foust (Ed.), Sodium-NaK engineering handbook, Gordon & Breach, New York, 1976.

[20] P. Li, E. Molina, K. Wang, X. Xu, G. Dehghani, A. Kohli, Q. Hao, M. H. Kassaee, S. M. Jeter, A. S. Teja, Thermal and transport properties of NaCl-KCl-ZnCl2 eutectic salts for new generation high-temperature heat-transfer fluids, Journal of Solar Energy Engineering 138 (2016) 054501–1–8.

[21] D. F. Williams, Assessment of Candidate Molten Salt Coolants for the NGNP/NHI Heat-Transfer Loop, Technical Report ORNL/TM-2006/69, Oak Ridge National Laboratory (ORNL), 2006.

[22] X. An, J. Cheng, P. Zhang, Z. Tang, J. Wang, Determination and evaluation of the thermophysical properties of an alkali carbonate eutectic molten salt, Faraday Discuss. 190 (2016) 327–338.

[23] J. T. Van Lew, P. Li, C. L. Chan, W. Karaki, J. Stephens, Analysis of heat storage and delivery of a thermocline tank having solid filler material, J. Sol. Energy Eng. 133 (2011) 021003.

[24] M. Y. Haller, C. A. Cruickshank, W. Streicher, S. J. Harrison, E. Andersen, S. Furbo, Methods to determine stratification efficiency of thermal energy storage processes - review and theoretical comparison, Solar Energy 83 (2009) 1847–1860.

[25] C. Xu, Z. Wang, Y. He, X. Li, F. Bai, Parametric study and standby behavior of a packed-bed molten salt thermocline thermal storage system, Renewable Energy 48 (2012) 1–9.

[26] D. A. Nield, A. Bejan, Convection in Porous Media, Springer New York, 2013.

[27] PPI Commodity Data for Industrial Chemicals, Bureau of Labor Statistics, accessed 15th March 2017.

[28] A. Fritsch, J. Flesch, V. Geza, C. Singer, R. Uhlig, B. Hoffschmidt, Conceptual study of central receiver systems with liquid metals as efficient heat transfer fluids, Energy Procedia 69 (2015) 644–653.

[29] Personal communication from SQM Europe M.V., October 2015.

[30] Industrial Minerals, accessed 15th June 2017. URL: `www.indmin.com`.

[31] USGS Mineral Yearbook, u.s. Geological Survey, accessed 15th February 2017. URL: `www.minerals.usgs.gov`.

[32] Alibaba, December 2016. URL: `www.alibaba.com`.

[33] K. Ismail, R. Stuginsky Jr, A parametric study on possible fixed bed models for PCM and sensible heat storage, Applied Thermal Engineering 19 (1999) 757–788.

[34] F. Incropera, T. Bergman, D. DeWitt, A. Lavine, Fundamentals of Heat and Mass Transfer, Wiley, 2013.

[35] K. S. Wakao, N., T. Funazkri, Effect of fluid dispersion coefficients on particle-to-fluid heat transfer coefficients in packed beds, Chemical Engineering Science 34 (1979) 325–336.

[36] B. Melissari, S. A. Argyropoulos, Development of a heat transfer dimensionless correlation for spheres immersed in a wide range of prandtl number fluids, International Journal of Heat and Mass Transfer 48 (2005) 4333–4341.

[37] S. Flueckiger, Z. Yang, S. V. Garimella, Thermocline energy storage in the solar one power plant: An experimentally validated thermomechanical investigation, in: ASME 2011 5th International Conference on Energy Sustainability, Parts A, B, and C, ASME, 2011.

[38] J.-F. Hoffmann, T. Fasquelle, V. Goetz, X. Py, A thermocline thermal energy storage system with filler materials for concentrated solar power plants: Experimental data and numerical model sensitivity to different experimental tank scales, Applied Thermal Engineering 100 (2016) 753–761.

[39] R. J. D. Tilley, Understanding solids : the science of materials, 2 ed., Wiley, Chichester [u.a.], 2013.